JOURNAL OF SPACECRAFT AND ROCKETS
Vol. 38, No. 6, November–December 2001

Interactions Between a Canard and Thick Bodies: Characteristics of the Components

Asher Sigal* and Michael Victor†
Technion—Israel Institute of Technology, 32000 Haifa, Israel

A modular model, consisting of cruciform canard controls mounted on a thin forebody and five interchangeable thick (larger-diameter) main bodies, was tested at a Mach number of 0.8. The canards were installed at the + and *x* positions and at deflection angles of 0, 6, and 12 deg. The model was equipped with two sting balances in a setup that enabled the obtaining of loads acting on the canard unit and those acting on the main bodies. The aerodynamic characteristics of the bodies alone and those of the canard unit are analyzed and compared with databases and predictions, respectively. A small effect of the thickening of the main bodies on the canard unit is observed.

Nomenclature

A	=	gain parameter in the model for vortex-induced normal-force coefficient
C_A	=	axial-force coefficient
C_{d_c}	=	crossflow drag coefficient
C_m	=	pitching-moment coefficient
C_{m_α}	=	pitching-moment curve slope
C_N	=	normal-force coefficient
C_{N_α}	=	normal-force curve slope
C_{pb}	=	base-pressure coefficient
D	=	diameter of main body, mm
D_B	=	base diameter, mm
d	=	diameter of forebody, mm
$K_{W(B)}$	=	wing in presence of body influence coefficient as a result of angle of attack
$k_{W(B)}$	=	wing in presence of body influence coefficient as a result of wing deflection
l	=	inclusive length of body, mm
l_{ab}	=	length of afterbody, mm
M	=	Mach number
S_M	=	main body cross-sectional area, $(\pi/4)D^2$, mm^2
S_P	=	body projection area, mm^2
S_R	=	reference area, $(\pi/4)d^2$, mm^2
x_{cp}	=	center of pressure location, relative to forebody-main body interface, mm
x'_{cp}	=	center of pressure location, relative to front end of boattail, mm
α	=	angle of attack
α_{eq}	=	equivalent angle of attack
α^v	=	threshold angle of attack in Eq. (5a)
δ	=	canard deflection
η	=	factor in the cross-flow method
φ	=	roll angle

Subscripts

bt	=	boattail
F	=	forebody (base contribution excluded)
f	=	front balance
m	=	main balance
1	=	thickening of main body
2	=	nonlinear (vortex induced) contribution

Superscript

$*$	=	coefficient based on S_M (main-body cross-sectional area)

Presented as Paper 97-2249 at the AIAA 15th Applied Aerodynamics Conference, Atlanta, GA, 23–25 June 1997; received 20 June 2000; revision received 1 April 2001; accepted for publication 23 April 2001.

*Adjunct Research Associate, Faculty of Aerospace Engineering; AsherS@aerodyne.technion.ac.il. Associate Fellow AIAA.

†Test Engineer, Wind Tunnel Laboratory, Faculty of Aerospace Engineering.

Introduction

SEVERAL guided weapon systems feature canard controls mounted on a thin forebody, which is attached to a thick main body (the maximum diameter of the main body is larger than that of the forebody). Typical examples are the configurations of the Paveway and guided bomb unit (GBU) families of guided bombs. See, for example, *Jane's Air-Launched Weapons*.[1]

According to aerodynamic theories, such as slender body theory (e.g., Ref. 2), the thickening or narrowing of a body causes a normal force at angles of attack. This has been shown from wind-tunnel results, such as Ref. 3. It is expected that, when canards are present upstream of diameter changes, the trailing vortices created by them will induce a downwash on the body, thus altering the distribution of the normal force. This effect can change the stability and control characteristics of the configuration. Despite the practical importance of this aerodynamic interaction, no systematic study of the effect was found.

Pitts, Nielsen, and Kaattari[4] (P-N-K), in their pioneering formulation of component buildup methodology, address the interaction between trailing vortices generated by a lifting surface and an afterbody having a variable diameter. They proposed an estimate for the change in the normal force, based on the effect of varying diameter on the lateral distance between the trailing vortices and their images. Nevertheless, most component buildup methodologies and codes do not consider this effect.

The overall objective of the present study was to investigate, both experimentally and analytically, the interaction between a canard and thick bodies. In particular, the analysis meant to find the accuracy of the P-N-K method and to improve it if necessary. The present part describes 1) wind-tunnel tests planned to establish a database; 2) the aerodynamic characteristics of the bodies alone and of the canard unit; and 3) identification of the effect of the main bodies on the canard unit.

Experimental Investigation

Models

The wind-tunnel modular model consists of a common forebody, five interchangeable main bodies, and a cruciform canard unit, as depicted in Fig. 1. The forebody is a hemisphere cylinder, having a diameter of 22 mm and fineness ratio of 6.0, yielding length of 132 mm. All of the main bodies have the same length (330 mm), but their diameters equal 1.5, 2.0, and 2.5 forebody diameters. Three of the main bodies are plain, i.e., they have cylindrical aft parts,

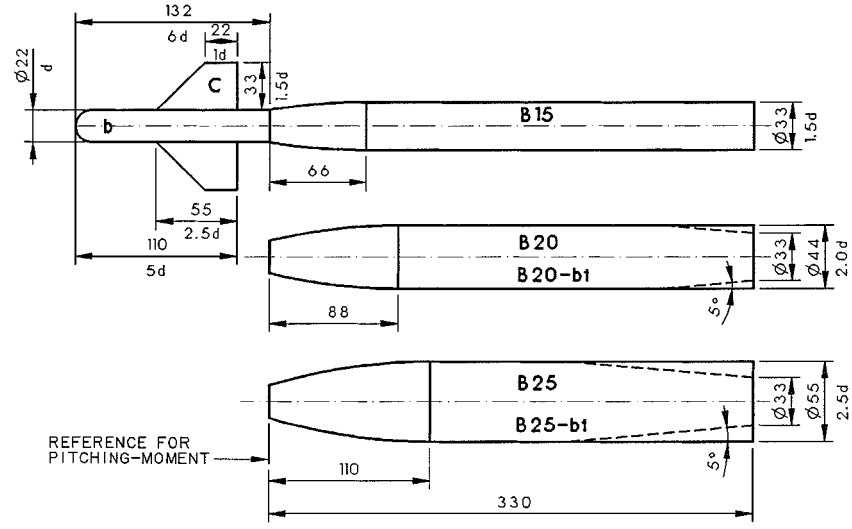

Fig. 1 Schematic of the model and designation of the modules.

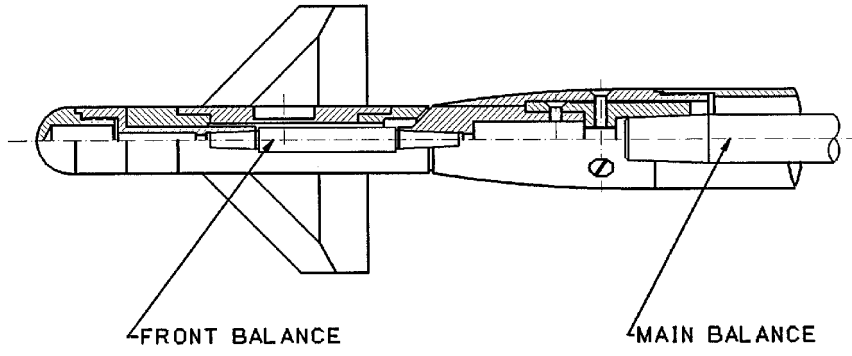

Fig. 2 General assembly of configuration b-C00-B15.

whereas the other two feature 5-deg boattails that end at the same base diameter ($D_B/d = 1.5$). The cruciform canards are mounted on the forebody. Their inclusive span is 88 mm, which equals 4.0 forebody diameters, the exposed aspect ratio is 1.71, the taper ratio is 0.4, and the leading edge is swept back 45 deg. The canard is removable and can be mounted at deflection angles of 0, 6, and 12 deg (leading-edge up). The hinge line is located 1.45 forebody diameters from the apex of the canards. The leading and trailing edges are beveled at 5 deg. A general assembly of the baseline configuration is shown in Fig. 2.

Each configuration is designated by b, indicating the forebody; B**, indicating main body diameter ratio; bt, indicating boattail; C** for the canard deflection angle; and + or x for the roll positions of the canards.

Wind-Tunnel and Test Conditions

The tests were carried out at the transonic wind tunnel (T1) of the Faculty of Aerospace Engineering of the Technion. This is a closed-cycle, ejector-driven facility, capable of operating at Mach numbers up to 1.16. The test section is 60 cm wide by 80 cm high, and the floor and the ceiling are perforated. For details see Ref. 5. The Mach number of the present tests was 0.8, and the Reynolds number, based on body length, was 6.5×10^6. The angle of attack was varied between -6 and 14 deg. Each body was tested alone, and in combination with the cruciform canards mounted at the three preset deflection angles, and at the two symmetrical roll positions, namely + and x.

Measurements

The main body was mounted on a six-component sting balance, as can be seen in Fig. 2. The forebody was mounted on a short five-component balance (no axial force). This arrangement provides the canard unit (forebody and canards) loads and the entire configuration loads, thus enabling the extraction of the canard on main-body interaction. Base pressure was measured in order to obtain the axial force, exclusive of the contribution of the base.

The accuracy of the normal force and the pitching moment obtained by both balances is 0.8% of the maximum loads measured in the present tests. The calibrations of the balances were verified by static loading after their installation in the wind tunnel.

Unless otherwise specified, the reference length and area for aerodynamic coefficients are forebody diameter and cross-sectional area, respectively. The reference point for pitching moments obtained by both balances is the interface plane between the forebody and the main bodies. These quantities are common to all configurations.

Results and Analysis 1: Bodies Alone

Sample Data

Samples of test data for the three plain bodies are shown in the two parts of Fig. 3. The coefficients obtained by each balance are plotted vs the respective angle of attack. In these tests the deflections of the front balance are very small, and the difference between forebody and main body angles of attack are less than 1%. Figure 3 shows that the normal-force and pitching-moment curves of the forebody are almost independent of the main bodies. As expected, the whole-body normal-force curves are higher for the thicker bodies, but the nonlinearity of these curves is smaller. Also, slopes of the pitching-moment curves of the thicker bodies are more negative, indicating a center-of-pressure location more to the rear.

Linear Characteristics

The normal-force and the pitching-moment curve slopes and the center-of-pressure locations were obtained by fitting straight lines to the linear sections of the C_N vs α, C_m vs α, and C_m vs C_N data, respectively. A typical range for the fit was ± 3 deg.

The contributions of the thickenings of the main bodies were obtained by subtracting the stability derivatives obtained by the front balance from those obtained by the main balance:

$$C_{N_\alpha 1} = C_{N_\alpha m} - C_{N_\alpha f} \tag{1a}$$

$$C_{m_\alpha 1} = C_{m_\alpha m} - C_{m_\alpha f} \tag{1b}$$

$$x_{\mathrm{cp}1}/d = C_{m_\alpha 1}/C_{N_\alpha 1} \tag{1c}$$

The normal-force curve slopes and the center-of-pressure locations of the front body, the whole plain bodies, and the thickenings are shown in the two parts of Fig. 4. Also shown are predictions based on slender-body theory[2]:

$$C_{N_\alpha} = 2(D/d)^2 \tag{2a}$$

$$C_{N_\alpha 1} = 2[(D/d)^2 - 1] \tag{2b}$$

The experimentally obtained normal-force curve slopes are about 15% higher than predicted. As expected, the center-of-pressure location is more aft as body thickness increases. The characteristics of the front body are practically independent of the main bodies.

For comparison purposes equivalent ogive-cylinder configurations having the same component and overall fineness ratios as the composed present bodies were defined. This definition is depicted in Fig. 5. Figure 6 compares the present results for the normal-force curve slopes with those of equivalent bodies. The databases for the comparison are the British ESDU[6] and Refs. 3 and 7. The present test data are only slightly smaller than those of the other sources, indicating that the fineness ratios are the key geometrical parameters that determine C_{N_α}.

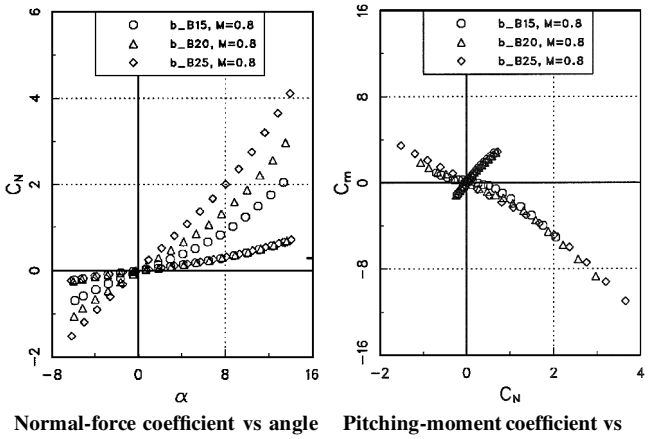

Normal-force coefficient vs angle of attack **Pitching-moment coefficient vs normal-force coefficient**

Fig. 3 Test results of the plain bodies.

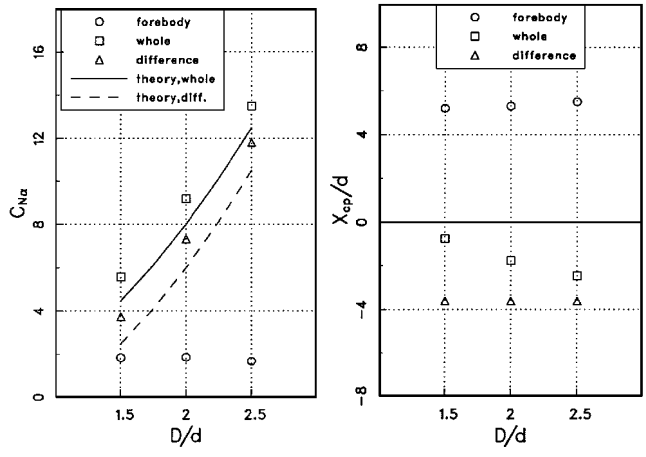

Normal-force curve slope **Center-of-pressure location**

Fig. 4 Linear characteristics of the plain bodies.

Effect of the Boattails

The contributions of the boattails to the stability derivatives were obtained by subtracting the stability derivatives of the plain bodies from those of the matching bodies that feature boattails. The findings are summarized in Table 1. The predicted values, based on slender-body theory,[2] are

$$C_{N_\alpha \mathrm{bt}} = 2[1.5^2 - (D/d)^2] \tag{3a}$$

$$C'_{m_\alpha \mathrm{bt}} = \tfrac{2}{3}[(D/d)^2 + 1.5(D/d) - 4.5](l_{\mathrm{ab}}/d) \tag{3b}$$

$$x'_{\mathrm{cp\,bt}}/d = C'_{m_\alpha \mathrm{bt}}/C_{m_\alpha \mathrm{bt}} \tag{3c}$$

The experimentally obtained normal-force curve slope of boattail B20 is 18% larger, in absolute value, than calculated by slender-body theory. For the larger boattail the agreement is very good.

Nonlinear Characteristics

The nonlinear contributions to the normal-force and the pitching-moment coefficient were obtained by subtracting the potential contribution from the data:

$$C_{N2} = C_N - \tfrac{1}{2}C_{N_\alpha} \sin 2\alpha \tag{4a}$$

$$C_{m2} = C_m - \tfrac{1}{2}C_{m_\alpha} \sin 2\alpha \tag{4b}$$

A study of these contributions shows that they only start past a threshold angle of attack. Hence, a model containing a threshold

Table 1 Characteristics of the boattails: bodies alone

Characteristic	b-B20-bt	b-B25-bt
$C_{N_\alpha \mathrm{bt}}$ (exp.)	−4.14	−7.8
$C_{N_\alpha \mathrm{bt}}$ (slender-body theory)	−3.5	−8.0
$x_{\mathrm{cp\,bt}}/d$ (exp.)	−12.6	−12.2
$x_{\mathrm{cp\,bt}}/d$ (slender-body theory)	−13.5	−11.9

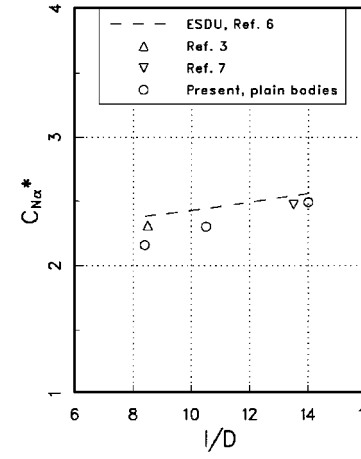

Fig. 6 Comparison of the normal-force curve slopes with those of equivalent bodies.

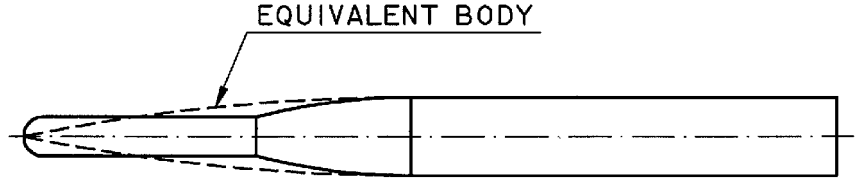

Fig. 5 Schematic of an equivalent body.

was selected to fit the data, as reasoned by Sigal[8]:

$$C_{N2} = A \sin^2(\alpha - \alpha^v), \qquad \alpha \geq \alpha^v \tag{5a}$$

$$x_{cp2}/d = C_{m2}/C_{N2} \tag{5b}$$

Equation (5a) is a modification of the prediction for the vortex-induced normal-force coefficient by the crossflow method by Allen and Perkins[9]:

$$C_{N2} = \eta(S_P/S_R)C_{d_c} \sin^2 \alpha \tag{6}$$

The parameters in Eqs. (5) were identified by fitting the models to the data obtained by Eqs. (4). The results are presented in the three parts of Fig. 7. The gain parameter A is 9–14% smaller than the projection to reference area ratio, indicating that (ηC_{d_c}) ranges between 0.91 and 0.86. The threshold angle of attack increases as diameter ratio increases, namely as fineness ratio decreases. The threshold angles of attack of the bodies with boattails are 2 deg smaller than those of the matching plain bodies. The center-of-pressure location of the vortex-induced normal-force coefficient, of the plain bodies, at angles of attack larger than 10 deg cluster about the center of the bodies. The center of pressure of the boattailed bodies is more to the rear. The findings are presented again in Fig. 8 as a function of whole-body fineness ratio and compared with a datum from Ref. 3. Note that A^* is related to C^*_{N2}, which is based on S_M. The gain parameter increases and the threshold angle of attack decreases as fineness ratio increases.

Axial Force

The forebody axial-force coefficient was obtained by subtracting the contribution of the base from the total axial force obtained by the main balance. The results are summarized in Table 2.

The boattails increase the base-pressure coefficient by about 0.1. In the case of b-B20, the boattail only slightly affects the axial-force coefficient, whereas in the case of b-B25 it reduces it considerably.

Results and Analysis 2: The Canard Unit

Characteristics of the Canard Unit

Test results of the canard unit mounted on body b-B20 at the + and the x positions are shown in Figs. 9 and 10, respectively. The coefficients were obtained by the front balance and are plotted vs forebody angle of attack. In the + position the normal-force curves of the deflected canards show stall at angles of attack of 12 and 8 deg, for deflection angles of 6 and 12 deg, respectively. The normal-force curves continue to increase past the stall zones. In the x position the normal-force curves neither stall nor cross over. However, the initial slopes decrease as the deflection angle increases. The slope of the pitching-moment curves decreases slightly as deflection angle increases, indicating a slightly more rearward center-of-pressure location. These findings are typical to all configurations.

The equivalent angle of attack that was introduced by Hemsch and Nielsen[10] and Hemsch[11] for one pair of canards, at roll angles

Table 2 Forebody axial-force coefficient and base pressure

Body		b-B15	b-B20	b-B25
Cylindrical afterbody	C_{A_F}	0.50	0.61	0.71
	C_{P_B}	−0.074	−0.076	−0.080
With boattail	C_{A_F}	——	0.62	0.65
	C_{P_B}	——	+0.027	+0.037

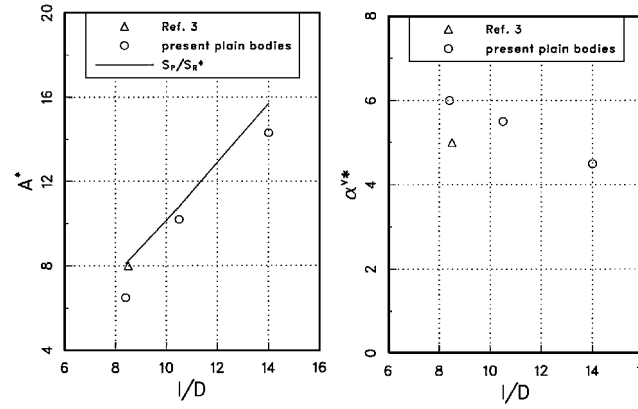

Gain parameter **Threshold angle of attack**

Fig. 8 Dependence of the nonlinear parameters on fineness ratio.

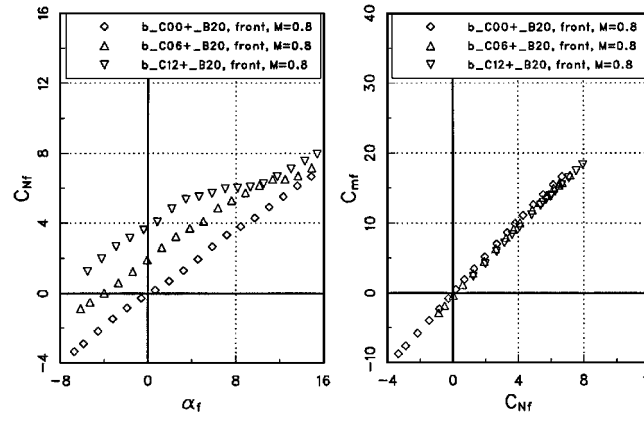

Normal-force coefficient vs angle of attack **Pitching-moment coefficient vs normal-force coefficient**

Fig. 9 Test results of the canard unit at the + position.

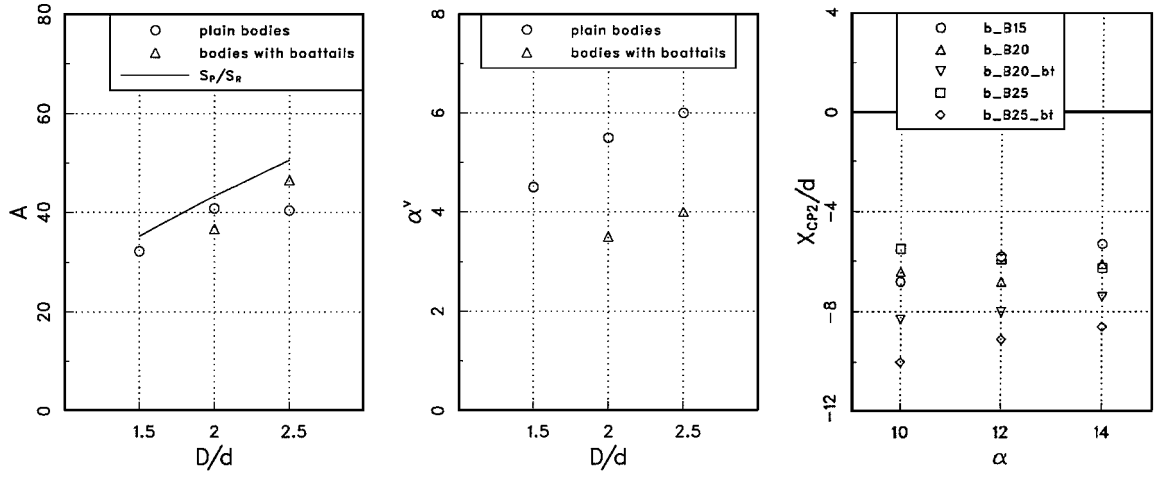

Gain parameter **Threshold angle of attack** **Center-of-pressure location**

Fig. 7 Nonlinear characteristics of the bodies.

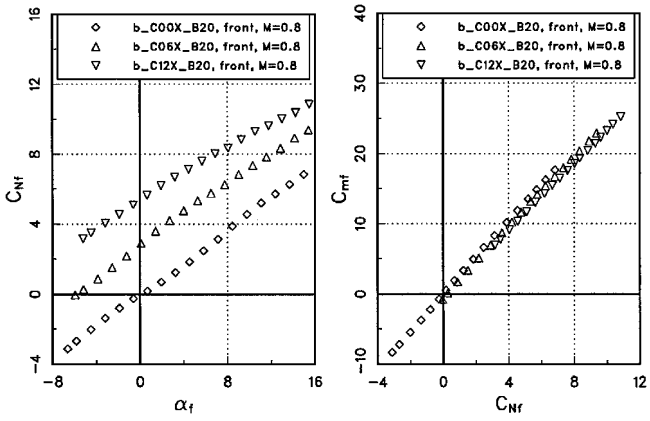

Normal-force coefficient vs angle of attack | Pitching-moment coefficient vs normal-force coefficient

Fig. 10 Test results of the canard unit at the x position.

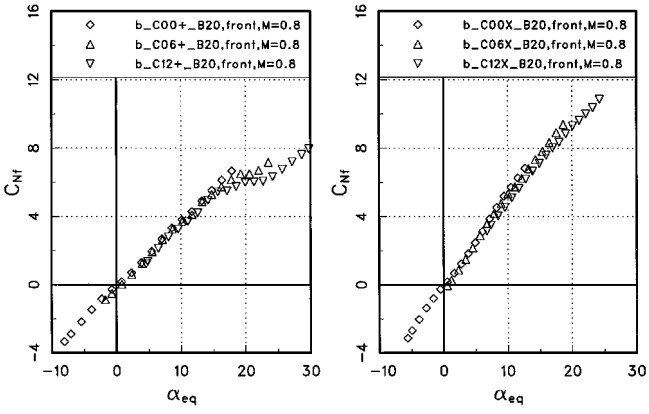

Canards at the + position | At the x position

Fig. 11 Dependence of the normal-force coefficient on equivalent angle of attack.

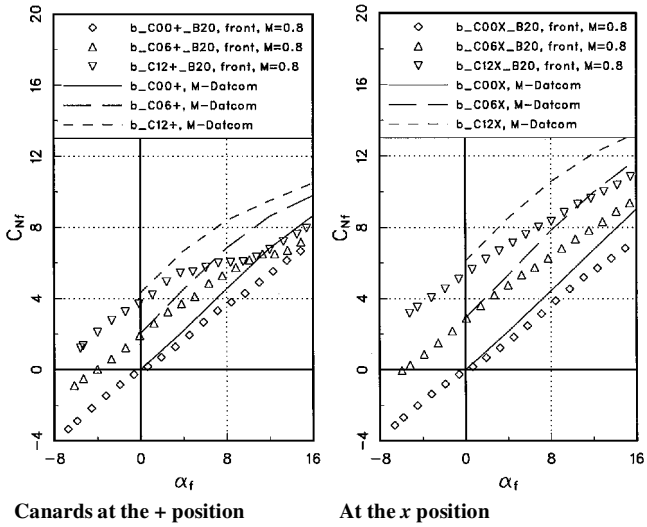

Canards at the + position | At the x position

Fig. 12 Comparison between predicted normal-force coefficient and test data.

of 0 and 45 deg, is

$$\alpha_{eq}(\varphi = 0) = K_{W(B)}\alpha + k_{W(B)}\delta \tag{7a}$$

$$\alpha_{eq}(\varphi = 45 \text{ deg}) = \sqrt{2}/2K_{W(B)}\alpha + k_{W(B)}\delta \tag{7b}$$

The values of the two influence coefficients were obtained from Ref. 4, and they are $K_{W(B)} = 1.20$ and $k_{W(B)} = 0.94$. The dependence of the normal-force coefficient upon the equivalent angles of attack is presented in Fig. 11. The curves for the three canard deflections are clustered. At the + position there is a plateau between equivalent angles of attack of 18 and 22 deg, indicating a stall. There is no

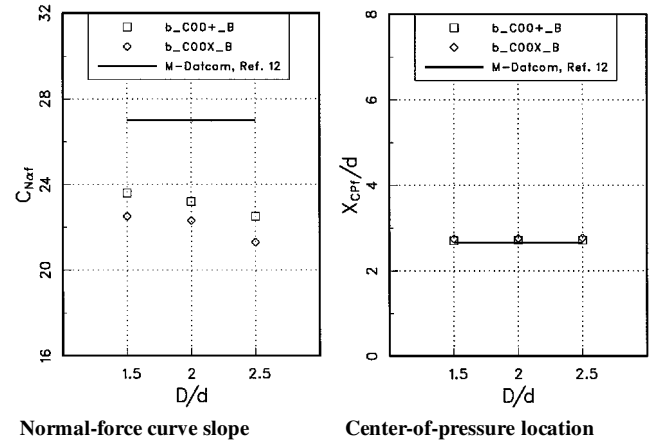

Normal-force curve slope | Center-of-pressure location

Fig. 13 Stability derivatives of the canard unit.

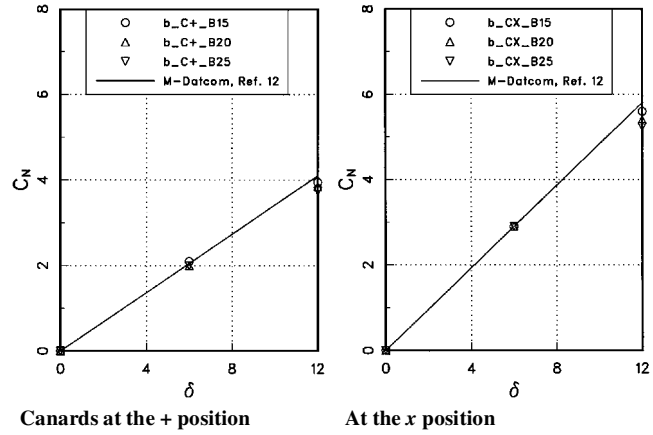

Canards at the + position | At the x position

Fig. 14 Canard normal-force coefficient as a result of canard deflection.

similar phenomenon in the x position. The initial slope of the curve at the x orientation is larger than that of the + position because the measured normal-force coefficient includes the contributions of the two pairs of canards.

Analysis

The aerodynamic characteristics of the canard unit were estimated using the 1997 version of the Missile Datcom code,[12] which is based on component buildup methodology. This code considers nonlinear effects from angle of attack and control deflection and uses empirical wing-body influence coefficients obtained by Burns and Bruns.[13] Comparisons between Missile-Datcom predictions and test data of the normal-force coefficient are shown in the two parts of Fig. 12. It is apparent that the Missile-Datcom overestimates the test data. The estimated normal-force curve slopes are larger than experimentally observed, and the prediction does not feature the saturation, caused by stall, that is observed with canards at the + position.

The experimental stability derivatives for the nondeflected canard were obtained as described in the preceding section. The results are presented in Fig. 13, in comparison with Missile-Datcom predictions. The experimentally obtained normal-force curve slope decreases slightly as body thickness increases. This effect is the first interaction observed. The code overestimates the test data by 14–20% at the + position and 20–27% at the x position. The center-of-pressure location is about independent of body thickness and is in very good agreement with the prediction. Figure 14 brings a comparison between predicted and experimentally obtained normal-force coefficient caused by canard deflection at zero angle of attack. Here too there is a slight decrease in the normal-force coefficient with increase of main-body to forebody diameter ratio. The agreement between Missile-Datcom estimate and test data is very good.

Conclusions

Wind-tunnel tests, at a Mach number of 0.8, of a modular model consisting of a cruciform canard unit and five interchangeable main

bodies, having different diameters, are described. Three of the main bodies have cylindrical afterbodies, whereas the other two feature boattails. A two-balance system enabled the identification of the aerodynamic loads acting on the canard unit and those acting on the main bodies.

Aerodynamic models, describing the linear and nonlinear characteristics of the bodies alone were obtained. The parameters in these models are in good agreement with available databases for similar bodies.

It is observed that the normal-force curve slope of the canard unit decreases slightly as main-body thickness increases.

The Missile-Datcom code overestimates the normal-force curve slope of the canard unit. The gap ranges between 14% for canards at the + orientation mounted on the thinnest body and 27% for canards at x on the thickest body. Good agreement was obtained for the normal-force coefficient caused by canard deflection.

Further analysis of the results and application to the analysis of missiles with canards are available in the second part of this article.

Acknowledgments

The Aerodynamics Laboratory of the Faculty of Aerospace Engineering of the Technion undertook the experimental part of this study. The authors are indebted to the late J. Rom for his interest in the study and for the support. W. Blake of the U.S. Air Force Research Laboratory, Air Vehicle Directorate, provided us with the Missile-Datcom code. Z. Rafael designed the wind-tunnel model. The paper was finalized during the first author's sabbatical visit to the Department of Aerospace Engineering, San Diego State University, San Diego, California.

References

[1] *Jane's Air-Launched Weapons*, edited by D. Lenox and A. Rees, Jane's Information Group Limited, Coulsdon, England, U.K., 1998, Sec. USA: Bombs, JALW-Issue 31.

[2] Nielsen, J. N., *Missile Aerodynamics*, Nielsen Engineering and Research, Inc., Mountain View, CA, 1988, pp. 66–74.

[3] Sigal, A., Yaacobi, A., and Avital, G., "The Effect of Afterbody Geometry on the Aerodynamic Characteristics of Circular Bodies," AIAA Paper 87-0444, Jan. 1987.

[4] Pitts, W. C., Nielsen, J. N., and Kaattari, G. E., "Lift and Center of Pressure of Wing-Body-Tail Combinations at Subsonic, Transonic, and Supersonic Speeds," NACA Rept. 1307, 1957.

[5] Salomon, M., Bracha, J., and Rom, J., "Characteristics of the 60 × 80 cm Induction Driven Close Return Transonic Wind Tunnel at the Aeronautical Research Center," *Israel Journal of Technology*, Vol. 8, Nos. 1–2, March 1970, pp. 111–118.

[6] "Normal Force, Pitching Moment and Side Force of Forebody-Cylinder Configurations for Angles of Attack Up to 90 Degree and Mach Numbers up to 5," ESDU International, Data Item 89014, London, Aug. 1989.

[7] Sigal, A., "Aerodynamic Effects of Body Roughness," *Journal of Spacecraft and Rockets*, Vol. 30, No. 3, 1993, pp. 298–303.

[8] Sigal, A., "Methods of Analysis and Experiments for Missiles with Noncircular Fuselages," *Tactical Missile Aerodynamics: Prediction Methodology*, edited by M. R. Mendenhall, Vol. 142, Progress in Astronautics and Aeronautics, AIAA , Washington, DC, 1992, pp. 171–223.

[9] Allen, H. J., and Perkins, E. W., "A Study of the Effect of Viscosity on Flow over Slender Inclined Bodies of Revolution," NACA Rept. 1048, 1951.

[10] Hemsch, M. J., and Nielsen, J. N., "Equivalent Angle-of-Attack Method for Estimating Nonlinear Aerodynamics of Missile Fins," *Journal of Spacecraft and Rockets*, Vol. 20, No. 4, 1983, pp. 356–362.

[11] Hemsch, M. J., "Component Build-Up Method for Engineering Analysis of Missiles at Low-to-High Angles of Attack," *Tactical Missile Aerodynamics: Prediction Methodology*, edited by M. R. Mendenhall, Vol. 142, Progress in Astronautics and Aeronautics, AIAA, Washington, DC, 1992, pp. 115–169.

[12] Blake, W. B., "Missile Datcom User's Manual—1997 Fortran 90 Revision," U.S. Air Force Research Lab., Air Vehicle Directorate, AFRL-VA-WP-1998-3009, Wright–Patterson AFB, OH, Feb. 1998.

[13] Burns, K. A., and Bruns, K. D., "Development of Improved Carryover Interference Method for Missile Datcom," AIAA Paper 96-3395, July 1996.

M. S. Miller
Associate Editor